Journal of Theoretical and Applied Mechanics, Sofia, 2016, vol. 46, No. 3, pp. 17–34

DE GRUYTER OPEN

SOLID MECHANICS

DOI: 10.1515/jtam-2016-0014

ENERGY AND TRANSMISSIBILITY IN NONLINEAR VISCOUS BASE ISOLATORS

Athanasios A. Markou, George D. Manolis

Laboratory for Statics and Dynamics, Department of Civil Engineering, Aristotle University, Thessaloniki 54124, Greece

e-mails: athanasiosmarkou@gmail.com, gdm@civil.auth.gr

[Received 30 May 2016. Accepted 20 June 2016]

Abstract. High damping rubber bearings (HDRB) are the most commonly used base isolators in buildings and are often combined with other systems, such as sliding bearings. Their mechanical behaviour is highly nonlinear and dependent on a number of factors. At first, a physical process is suggested here to explain the empirical formula introduced by J.M. Kelly in 1991, where the dissipated energy of a HDRB under cyclic testing, at constant frequency, is proportional to the amplitude of the shear strain, raised to a power of approximately 1.50. This physical process is best described by non-Newtonian fluid behaviour, originally developed by F.H. Norton in 1929 to describe creep in steel at high-temperatures. The constitutive model used includes a viscous term, that depends on the absolute value of the velocity, raised to a non-integer power. The identification of a three parameter Kelvin model, the simplest possible system with nonlinear viscosity, is also suggested here. Furthermore, a more advanced model with variable damping coefficient is implemented to better model in this complex mechanical process. Next, the assumption of strain-rate dependence in their rubber layers under cyclic loading is examined in order to best interpret experimental results on the transmission of motion between the upper and lower surfaces of HDRB. More specifically, the stress-relaxation phenomenon observed with time in HRDB can be reproduced numerically, only if the constitutive model includes a viscous term, that depends on the absolute value of the velocity raised to a non-integer power, i. e., the Norton fluid previously mentioned. Thus, it becomes possible to compute the displacement transmissibility function between the top and bottom surfaces of HDRB base isolator systems and to draw engineering-type conclusions, relevant to their design under time-harmonic loads.

Key words: Base isolation, high damping rubber bearings (HDRB), nonlinear viscosity, transmissibility function, energy dissipation

*Corresponding author e-mail: gdm@civil.auth.gr

1. Introduction

As suggested by the results of recent research efforts [1, 2], the strain-rate dependence in HDRB is governed by a nonlinear viscosity term. This non-Newtonian fluid behavior is described by the model developed originally by Norton [3] to describe creep in steel at high-temperatures, see also Irgens [4] and Besson et al. [5]. Another interesting conclusion is that the rate-independent part of the model simply consists of an elastic spring, see also Dall' Asta and Ragni [6].

As highlighted by Kelly and coworkers, see [7] and [8], based on empirical observations of several cyclic tests under constant frequency on elastomeric isolators, the dissipated energy per cycle W_D is proportional to the amplitude of the shear displacement u_0 raised to an exponent of approximately 1.50. They concluded that no fundamental physical process that leads to a constant near 1.50 has been identified. Actually, the physical process that leads to an exponent on the shear strain amplitude is the non-Newtonian fluid behavior i.e., the nonlinear viscous behavior of a Norton fluid.

According to Kelly [9], the transmissibility function (TR) defined as the ratio between output and input in a base isolation (BI) system with rubber-like materials can be expressed either in terms of linear viscosity or in terms of hysteretic damping. The novelty of the present work is to formulate and compute the TR function of rubber-like BI materials by taking into account the aforementioned nonlinear viscosity and demonstrating that this function best fits available experimental results. For this reason, we investigate how the TR function is affected by two key parameters of the nonlinear viscous element, namely the damping ratio ζ and the exponent n on the velocity term. We suggest the best combination, over a wide range of frequency ratio values, of these two parameters in order to reduce the magnitude of the TR function, which is important information regarding the industrial design of BI systems with optimum use of the constituent materials. An HDRB consists of alternating layers of rubber components, natural or synthetic, with intervening thin steel plates and its dimensions vary anywhere from 0.30 m to around 1.50 m, depending on the design considerations decided upon by the manufacturer. These isolators are custom-made and their cost is an important parameter in their adoption for seismic isolation purposes in conventional buildings.

2. The high damping rubber bearings physical model

The physical model for HDRB isolators comprises a linear elastic spring of stiffness k and a nonlinear viscous damper with damping coefficient c_n and

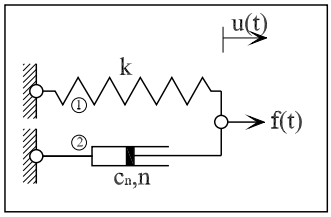

Fig. 1. Kelvin model with nonlinear viscosity.

exponent n, see Fig. 1. The constitutive equations of the two element system are defined as follows:

$$f_1(t) = k\ u(t); \quad f_2(t) = c_n\ |\dot{u}(t)|^n\ \text{sign}(\dot{u}(t)); \quad n \geq 0, \tag{1}$$

where sign is the signum function. The force that develops in the system is equal to:

$$f(t) = f_1(t) + f_2(t). \tag{2}$$

The dissipated energy per one cycle of vibration W_D according to Naeim and Kelly [10], is defined as:

$$W_D = c_o\ u_0^{a_o}, \tag{3}$$

where u_0 is the displacement amplitude and a_o, c_o are constants. The displacement and velocity of the system under cyclic tests are provided by the following expressions:

$$u(t) = u_0\ \sin(\omega t); \quad \dot{u}(t) = \omega u_0\ \cos(\omega t); \quad \omega = \frac{2\pi}{T}, \tag{4}$$

where T is the period of the cyclic test. Next, the dissipated energy W_D^C by the nonlinear viscous element over a cycle of harmonic motion will be equal to:

$$W_D^C = \int_0^{\frac{2\pi}{\omega}} f_2(t)\dot{u}(t)dt. \tag{5}$$

By substituting Eq. (4) to Eq. (5) we get the following result:

$$W_D^C = c_n \left[\omega^{n+1} \int_0^{\frac{2\pi}{\omega}} |\cos(\omega t)|^{n+1}\, dt\right] u_0^{n+1}. \tag{6}$$

Using the symmetry of the cosine function gives:

$$W_D^C = c_n \left[4\omega^{n+1} \int_0^{\frac{\pi}{2\omega}} (\cos(\omega t))^{n+1}\, dt \right] u_0^{n+1}. \tag{7}$$

By setting $x = \omega t$ obtain that:

$$W_D^C = c_n \left[4\omega^{n} \int_0^{\frac{\pi}{2}} (\cos(x))^{n+1}\, dx \right] u_0^{n+1}. \tag{8}$$

Finally, the analytical solution of the dissipated energy per cycle of the nonlinear viscous element by using the Wallis cosine formula [11], see also Soong and Constantinou [12], is equal to:

$$W_D^C = c_n \left[4\sqrt{\pi} \frac{\omega^n}{(n+1)} \frac{\Gamma\left(\frac{1}{2}\,(n+2)\right)}{\Gamma\left(\frac{1}{2}\,(n+1)\right)} \right] u_0^{n+1}, \tag{9}$$

where Γ is the Gamma function. By equating Eq. (3) with Eq. (9) we get:

$$n = a_o - 1; \quad c_n = \frac{c_o}{\left[4\sqrt{\pi} \frac{\omega^n}{(n+1)} \frac{\Gamma\left(\frac{1}{2}\,(n+2)\right)}{\Gamma\left(\frac{1}{2}\,(n+1)\right)} \right]}. \tag{10}$$

An improvement over the Kelvin system with nonlinear viscosity would be to include displacement amplitude dependence in the damping coefficient c_n. By replacing c_n in Eq. (9) with a linear displacement amplitude function as:

$$c_n = p_1 + p_2\, u_0, \tag{11}$$

gives the dissipated energy in the form:

$$W_D^L = (p_1 + p_2\, u_0) \left[4\sqrt{\pi} \frac{\omega^n}{(n+1)} \frac{\Gamma\left(\frac{1}{2}\,(n+2)\right)}{\Gamma\left(\frac{1}{2}\,(n+1)\right)} \right] u_0^{n+1}. \tag{12}$$

3. Computation of energy in the high damping rubber bearings isolators

A set of cyclic shear tests under constant frequency were recently conducted on a HDRB by Markou et al. [2] and the log-log plot of the energy W_D vs displacement amplitude u_0 is shown in Fig. 2. The height of the rubber in the HDRB was 96 mm and 10 cyclic tests under a constant frequency of

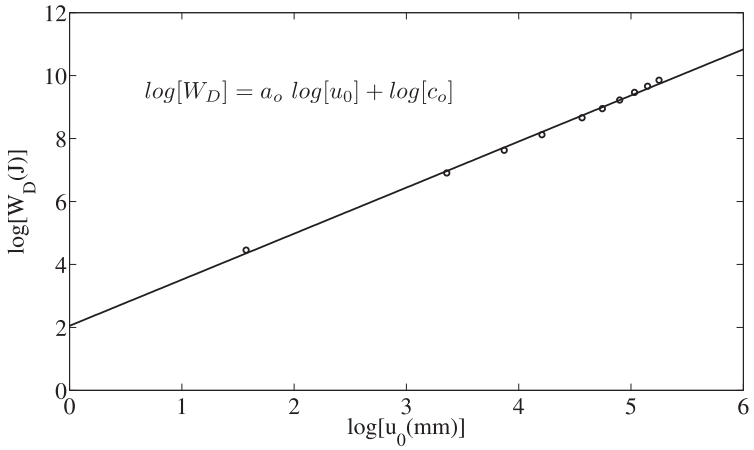

Fig. 2. Energy dissipation characteristics of HDRB isolators

0.50 Hz were implemented with the amplitude of the shear strain ranging from $\gamma = 0.05$ to $\gamma = 2$. The average normalized error in the calculated dissipated energy, using the proposed numerical models W_D^m against the experimentally obtained value W_D quantified, as:

$$e = \sqrt{\frac{1}{N}\sum_{i=1}^{N}\left[\frac{W_D(i) - W_D^m(i)}{W_D(i)}\right]^2}; \quad N = 10, \tag{13}$$

where N is the number of the tests. The numerical values used for the problem parameters a_o and c_o of Eq. (3) were obtained by fitting a straight line in the energy-displacement log-log graph and are presented in Table 1, see also Fig. 2. The set of identified parameters for the Kelvin model with constant damping and the ones for variable damping are also presented in Table 1. The optimization algorithm developed by Hansen [13] was used in order to minimize Eq. (13) and obtain the parameter values for the Kelvin model with variable damping. In Table 2, the experimentally measured energy W_D, the identified energy for the Kelvin model with constant and variable damping coefficients, namely W_D^C and W_D^L, as obtained for ten different levels of strain amplitudes are all listed, see also Fig. 3. The stiffness k in the Kelvin models for all cases was obtained in order to match the initial slope in the experimentally obtained strain-stress curves.

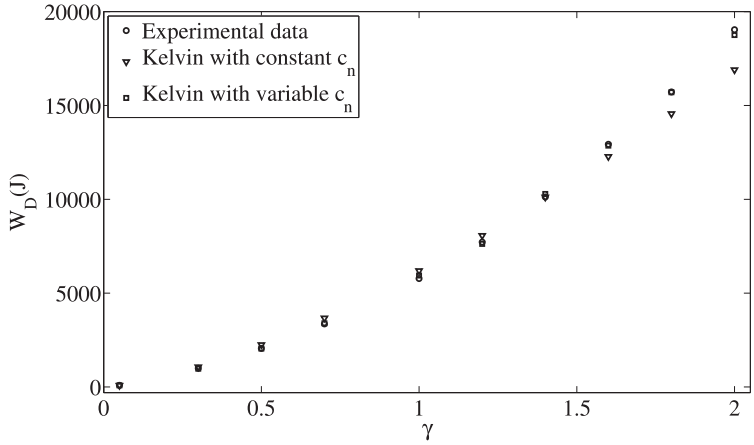

Fig. 3. Experimental and numerically simulated energy dissipation using the Kelvin model with constant and variable damping coefficients c_n

Table 1. Experimentally identified parameters a_o, c_o, values for the Kelvin model with constant and variable damping coefficients

Parameters a_o, c_o				
a_o		c_o $(\mathrm{kNmm^{1-a_o}})$		
1.464		7.763		
Kelvin model with constant damping coefficient				
n		c_n $\left(\mathrm{kN}\left(\frac{\mathrm{sec}}{\mathrm{mm}}\right)^{\mathrm{n}}\right)$		k $\left(\frac{\mathrm{kN}}{\mathrm{mm}}\right)$
0.464		1.656		0.700
Kelvin model with variable damping coefficient				
n	p_1 $\left(\mathrm{kN}\left(\frac{\mathrm{sec}}{\mathrm{mm}}\right)^{\mathrm{n}}\right)$		p_2 $\left(\mathrm{kN}\frac{\mathrm{sec}^{\mathrm{n}}}{\mathrm{mm}^{\mathrm{n+1}}}\right)$	k $\left(\frac{\mathrm{kN}}{\mathrm{mm}}\right)$
0.299	2.1254		0.0097	0.700

Table 2. Experimental (W_D) and computationally identified (W_D^C, W_D^L) energy dissipation values for different levels of strain amplitude γ

γ	0.05	0.30	0.50	0.70	1.00	1.20	1.40	1.60	1.80	2.00	$e(\%)$
$W_D(J)$	86	998	2054	3364	5778	7721	10126	12928	15718	19039	
$W_D^C(J)$	78	1062	2245	3672	6191	8065	10112	12275	14555	16897	7.68
$W_D^L(J)$	87	975	2046	3394	5940	7622	10284	12859	15702	18752	1.49

4. Equation of motion for the high damping rubber bearings isolator

The simplified model, that will be considered for the present study for the HDRB, is a single degree of freedom (SDOF) system, see Fig. 4. This mechanical model consists of a linear elastic spring with stiffness k (element 1) and a nonlinear viscous damper (element 2) with damping coefficient c_n and exponent n on the absolute value of the velocity. The constitutive equations were given by Eq. (1). For seismically induced motions, we distinguish between the absolute and relative displacements of the SDOF system, representing the base isolation (BI) system. These are defined as follows in terms of the input ground motion (subscript g):

$$u^t(t) = u(t) + u_g(t); \quad u(t) = u^t(t) - u_g(t). \tag{14}$$

The equation of motion of the BI system can now be written

$$m\ \ddot{u}(t) + c_n\ |\dot{u}(t)|^n\ \text{sign}(\dot{u}(t)) + k\ u(t) = P(t), \tag{15}$$

where:

$$P(t) = -m\ \ddot{u}_g(t). \tag{16}$$

The BI system will be excited by harmonic ground motion, as this is a stringent test in the case of seismically-induced motions. This harmonic ground motion and its time derivatives are given by:

$$u_g(t) = \tilde{u}_g\ \sin(\omega\ t); \quad \dot{u}_g(t) = \omega\ \tilde{u}_g\ \cos(\omega\ t); \quad \ddot{u}_g(t) = -\omega^2\ \tilde{u}_g\ \sin(\omega\ t), \tag{17}$$

where $\tilde{u}_g$ is the amplitude of the seismic motion. Finally, the equation of motion becomes:

$$\ddot{u}(t) + 2\ \zeta\ v_r\ \omega_0\ |\dot{u}(t)|^n\ \text{sign}(\dot{u}(t)) + \omega_0^2\ u(t) = \omega^2\ \tilde{u}_g\ \sin(\omega\ t), \tag{18}$$

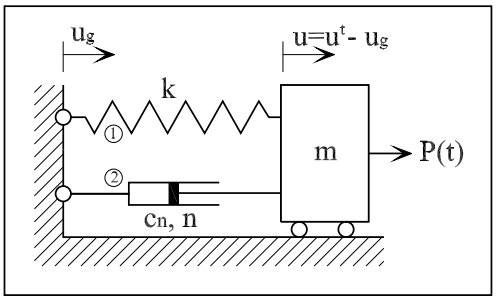

Fig. 4. SDOF HDRB base isolation system with a nonlinear viscosity element

where

$$\zeta = \frac{c_n}{2\ m\ \omega_0\ v_r}; \quad \omega_0 = \sqrt{\frac{k}{m}}; \quad v_r = 1\left(\frac{m}{sec}\right)^{1-n}. \tag{19}$$

It is worth noticing, that the damping ratio ζ is defined as the ratio of the actual damping in the system divided by the critical damping at $n = 1$.

5. Equation of motion state-space formulation

Equation (18) will be solved by using the state-space formulation, as it is a nonlinear differential equation of the second order, for which analytical solutions are possible only under certain restrictions (e. g., for exponent $n = 1$). Let us assume a kinematic vector $\mathbf{V}$, defined as follows:

$$\mathbf{V} = \left\{ \begin{array}{c} u(t) \\ \dot{u}(t) \end{array} \right\}. \tag{20}$$

The first derivative of the the vector $\mathbf{V}$ is given by:

$$\begin{aligned} \dot{\mathbf{V}} &= \left\{ \begin{array}{c} \dot{u}(t) \\ \ddot{u}(t) \end{array} \right\} \\ &= \left\{ \begin{array}{c} \dot{u}(t) \\ \omega^2\ \tilde{u}_g\ \sin(\omega\ t) - 2\ \zeta\ v_r\ \omega_0\ |\dot{u}(t)|^n\ \mathrm{sign}(\dot{u}(t)) - \omega_0^2\ u(t) \end{array} \right\}. \end{aligned} \tag{21}$$

The solution of Equation (21) will be implemented by the use of first-order differential equation solvers available in the software package Matlab [14]. The absolute displacement TR function amplitude is defined as:

$$TR = \frac{\tilde{u}^t}{\tilde{u}_g}, \tag{22}$$

where $\tilde{u}^t$ is the amplitude of the absolute displacement. The TR function for the special case of $n = 1$ is expressed by the following equation, see Kelly [9]:

$$TR_{(n=1)} = \frac{\tilde{u}^t}{\tilde{u}_g} = \sqrt{\frac{1 + (2\ \zeta\ \Omega)^2}{[1 - \Omega^2]^2 + [2\ \zeta\ \Omega]^2}}; \quad \Omega = \frac{\omega}{\omega_0}. \tag{23}$$

6. Numerical results for the transmissibility function

The numerical results will be given in three parts. In the first part, the effect of damping ratio ζ on the trasmissibility function TR, under constant exponent n will be investigated. In the second part, the dependence of the TR on the exponent n on TR, under constant damping ratio ζ will be investigated. In the last part, characteristic points drawn from these graphs will be identified and presented.

6.1. Transmissibility function for variable damping ratio ζ

The frequency ratio increment $\Delta\Omega$ used in the computations involving Eq. (22) is equal to 0.01, while the range of the frequency ratio Ω varies from zero to three. In Fig. 5 (a), the absolute displacement transmissibility function TR is plotted against frequency ratio Ω in logarithmic scale for different levels of damping ratio ζ, at a constant value of exponent $n = 0.20$. At the first characteristic point d (to be formally defined in a next sub-section) of Fig. 5 (a), the trasmissibility is $TR = 0.92$ at $\Omega = 1.44$ and is independent of the damping ratio ζ. For frequency ratios smaller than d, namely 1.44, an increase in damping reduces the TR. The opposite is true for frequency ratios larger than 1.44, where an increase in damping increases the TR. In Table 3, we list the maximum values of the TR, at resonance, for all damping ratios and $n = 0.20$. It is obvious from the results, that damping is beneficial at resonance, since it can reduce TR from infinity at $\zeta = 0$ to 1.21 at $\zeta = 0.50$. It might be interesting to notice that for damping ratios larger than $\zeta = 0.30$, resonance does not occur at $\Omega = 1$.

In Fig. 5 (b), the absolute displacement TR is presented at a constant exponent n value equal to 0.40. At the characteristic point d with $\Omega = 1.43$,

Table 3. Maximum absolute values for the displacement TR function for variable damping ratio ζ and exponent n

	ζ	0	0.05	0.10	0.20	0.30	0.40	0.50	1
n=0.20	max(TR)	∞	307.18	184.42	36.09	5.34	1.85	1.21	1
	Ω	1	1	1	1	1.01	1.08	1.18	0.59
n=0.40	max(TR)	∞	143.95	39.30	7.16	2.81	1.66	1.27	1
	Ω	1	1	1	1	1.03	1.07	1.11	0.82
n=0.60	max(TR)	∞	39.78	12.70	4.13	2.28	1.61	1.33	1.03
	Ω	1	1	1	1	1.01	1.02	1.03	0.97
n=0.80	max(TR)	∞	16.86	7.14	3.16	2.07	1.62	1.39	1.08
	Ω	1	1	1	0.98	0.98	0.95	0.91	0.83
n=1.00	max(TR)	∞	10.05	5.12	2.73	1.99	1.66	1.47	1.15
	Ω	1	1	0.99	0.96	0.93	0.89	0.86	0.71

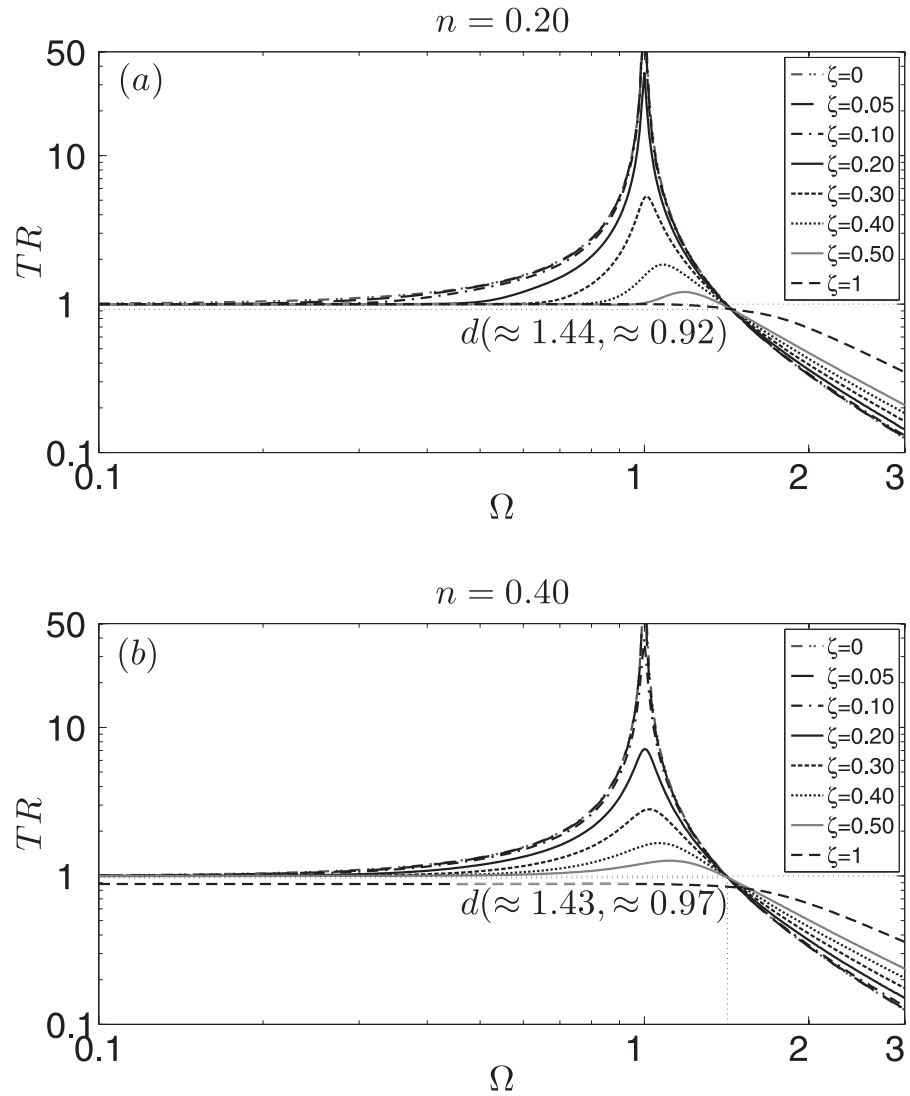

Fig. 5. Transmissibility function for harmonic excitation and variable damping ζ with exponent values (a) $n = 0.20$, (b) $n = 0.40$

the TR is equal to 0.97 and is again independent from the damping ratio ζ. For frequency ratios lower than 1.43, increase in the damping ratio reduces the TR, while the opposite holds true for frequency ratios larger than 1.43. In Table 3, the maximum values of TR at resonance, are also given for all damping ratios and for $n = 0.40$. As in the previous case, the results show how effective damping is at resonance, since it can reduce TR from infinity at $\zeta = 0$ to 1.27 at $\zeta = 0.50$.

Next, Figs 6 (a) and 6 (b) plot the absolute displacement TR against frequency ratio Ω for different levels of damping ratio ζ at constant exponent n values equal to 0.80 and 1, respectively. At the characteristic point d with frequency ratio of $\sqrt{2}$, the TR is equal to 1 and is independent of damping. For frequency ratios lower than $\sqrt{2}$, an increase in damping, reduces the TR, while for frequency ratios larger than $\sqrt{2}$, the opposite holds true. Finally, Table 3 summarizes the maximum values of TR, at resonance, for all damping ratios and for $n = 0.20$, 0.40, 0.60, 0.80 and 1.

6.2. Transmissibility function for variable exponent n

In Fig. 7 (a) the TR is plotted versus frequency ratio Ω in logarithmic scale, for constant damping ratio ζ, equal to 0.05 and for variable exponent n. For this level of damping, the transmissibility, apart at resonance, changes little for different values of exponent n. Two characteristic points are shown in the graph, namely a and b, that will shortly be discussed in more detail in what follows. In-between points a and b, the lower the value of n is, the larger the TR becomes. Reduction of exponent n is beneficial for a frequency ratio lower than a, namely 0.76, and for a frequency ratio larger than b, namely $\sqrt{2}$. In this case, reduction of n reduces the values of TR.

In Fig. 7 (b), the TR is presented against frequency ratio Ω for constant damping ratio ζ equal to 0.10. At this level of damping, the transmissibility changes for different values of exponent n. In-between characteristic points a and b, the lower the value of n is, the larger the TR becomes. Reduction of exponent n is beneficial for frequency ratios lower than a, namely 0.78, and for frequency ratios larger than b, namely $\sqrt{2}$. In this case, reduction of n reduces the values of TR. In Fig. 8 (a), the TR is presented against Ω for constant damping ratio ζ equal to 0.40. Once more, in-between characteristic points a and b, the lower the value of n is, the larger the TR becomes. Reduction in n is beneficial for frequency ratios lower than a, namely 1, and for frequency ratios larger than b, namely $\sqrt{2}$. In this case, a reduction in n reduces the values of TR. Finally, in Fig. 8 (b), the TR is presented for constant damping ratio ζ equal to 1, i. e., at critical damping. In this case, there are no characteristic

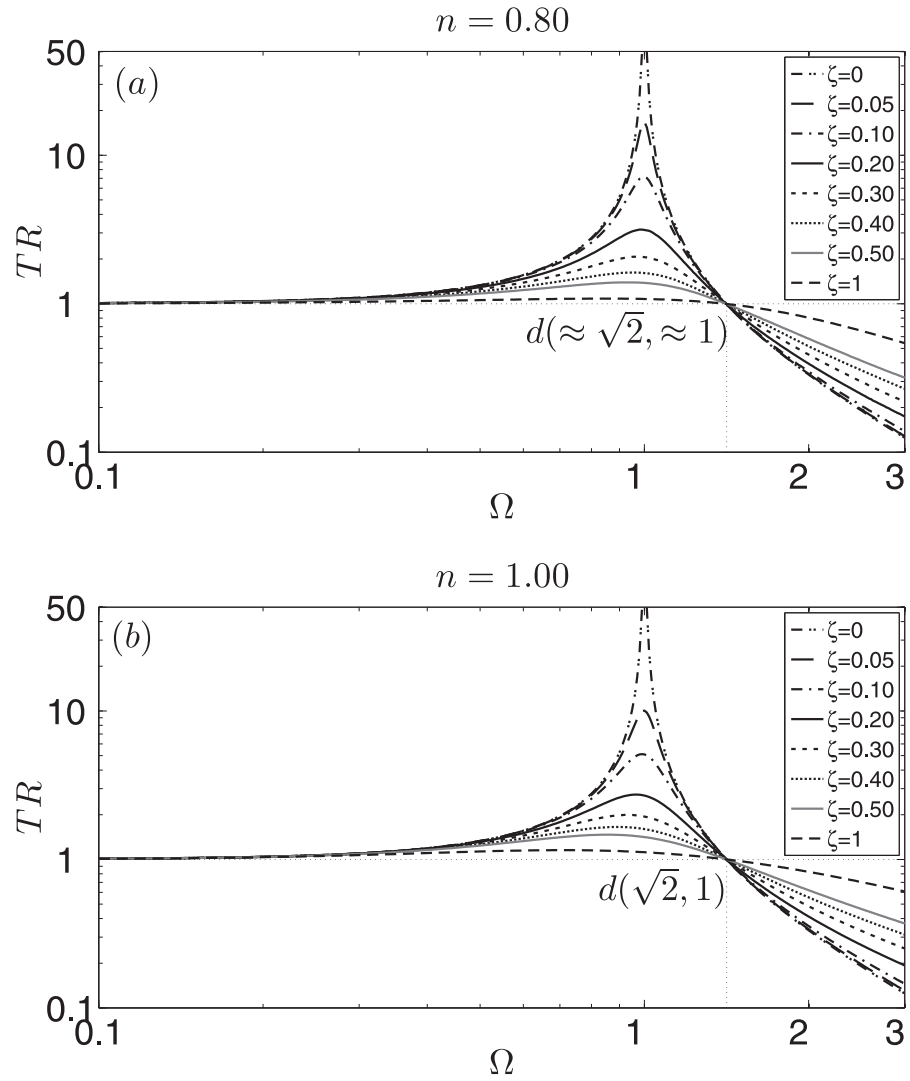

Fig. 6. Transmissibility function for harmonic excitation and variable damping ζ with exponent values (a) $n = 0.80$ and (b) $n = 1.00$

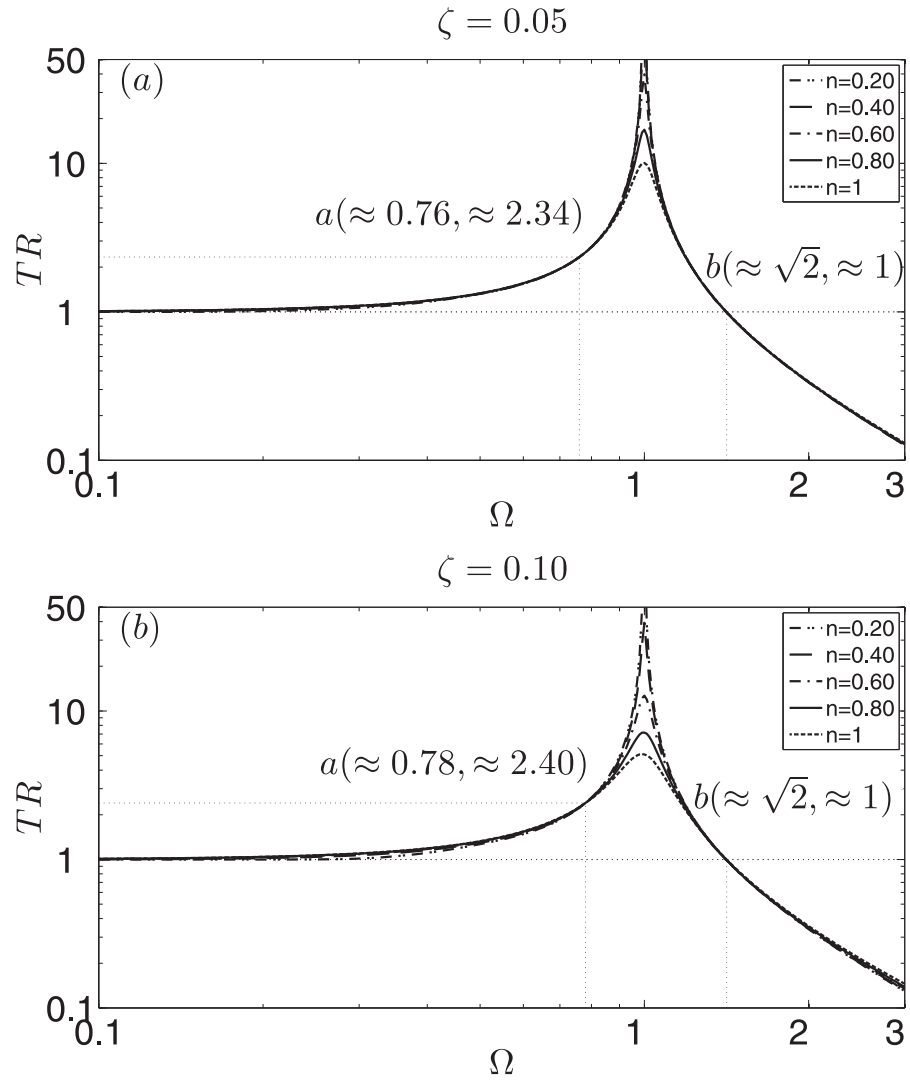

Fig. 7. Transmissibility function for harmonic excitation for varying exponent n with constant damping value (a) $\zeta = 0.05$, (b) $\zeta = 0.10$

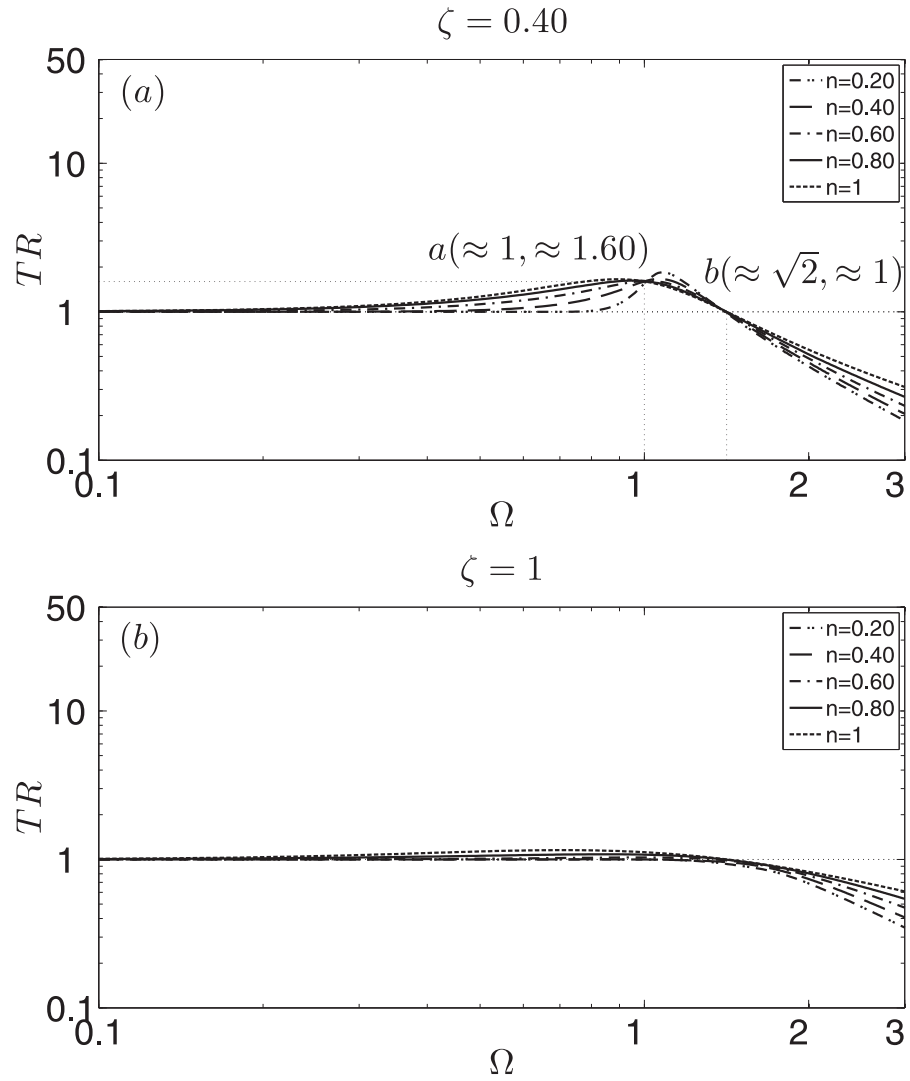

Fig. 8. Transmissibility function for harmonic excitation for varying exponent n with constant damping value (a) $\zeta = 0.40$ and (b) $\zeta = 1$

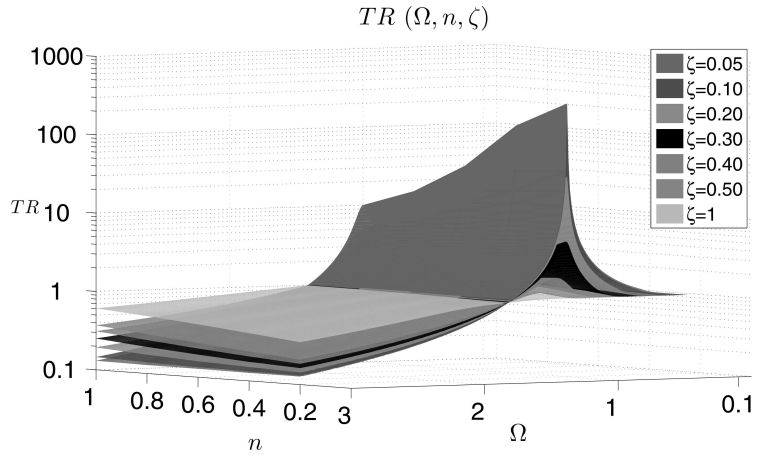

Fig. 9. Variation of the transmissibility function TR as a function of the frequency ratio Ω with damping ratio ζ and exponent n

points to be defined and the smaller the exponent n becomes, the smaller the TR is. In sum, all previously listed results are best summarized in the three-dimensional plot of Fig. 9.

6.3. Characteristic points *a*, *b* and *d*

As seen in Figs 7 and 8, the characteristic point b is always the same for all levels of damping ratio ζ, namely equal to $(\sqrt{2}, 1)$. The opposite is true for characteristic point a. As the damping ratio increases, point a increases up to a damping ratio of $\zeta = 0.45$, see Fig. 10 (a). For damping ratios up to 0.45, the relationship between point a and the damping ratio can be expressed as follows:

$$\zeta = -3.40\ \Omega^2 + 7.45\ \Omega - 3.64. \tag{24}$$

It is worth pointing out that for damping level equal to zero, the TR is independent of exponent n, because this term vanishes.

In Fig. 10 (b), the variation of characteristic point d is presented for different values of exponent n. The relation between point d and the exponent n is expressed by the following equation for n ranging from 0 to 0.60:

$$n = -284.29\ \Omega^2 + 795.92\ \Omega - 556.42. \tag{25}$$

For values of exponent n larger than 0.60, critical point d is constant and equal to $\sqrt{2}$.

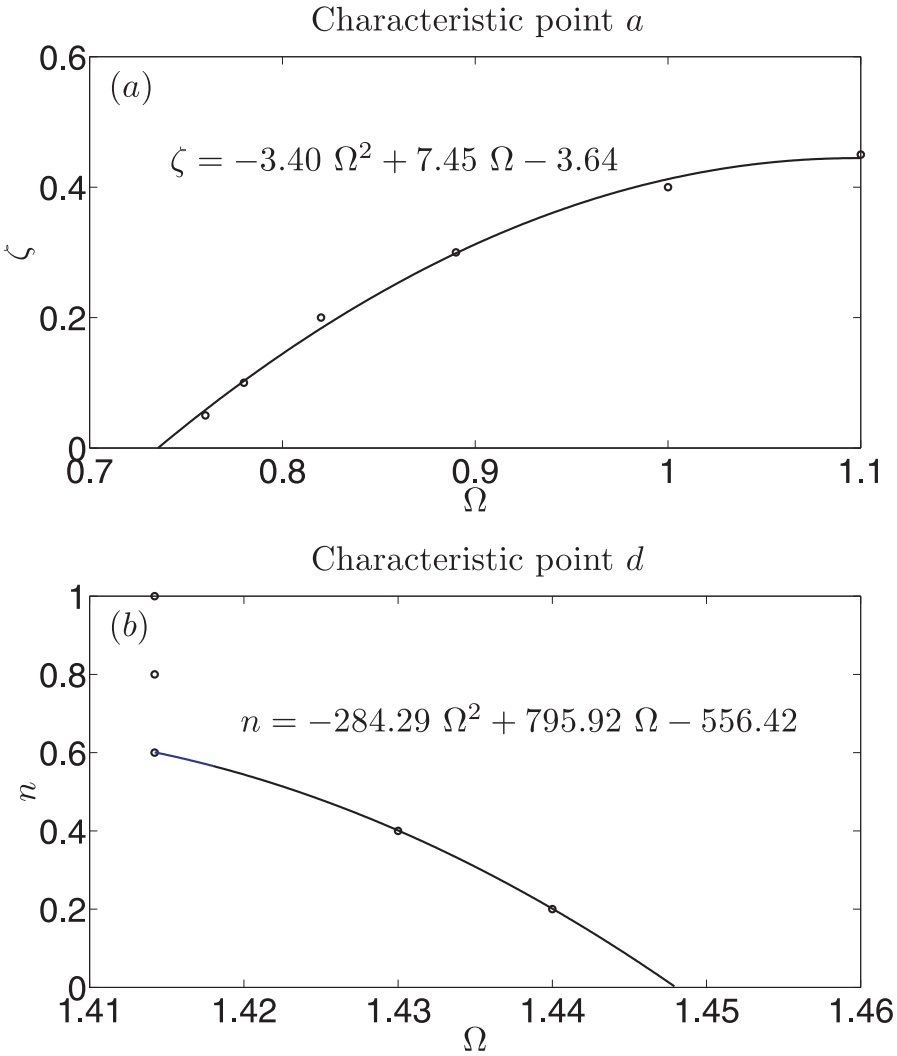

Fig. 10. Variation of the characteristic points (a) a and (b) d according to different levels of damping ratio ζ and exponent n

7. Conclusions

In this work, a physical mechanism with nonlinear viscosity is suggested for the description of energy dissipation in HDRB, under cyclic testing at constant frequency. At the same time, an analytical solution for energy dissipated by the nonlinear viscous element under cyclic testing is provided. At first, a simple Kelvin model incorporating the nonlinear viscous element is used and numerical results indicate an error of about 8%, see Table 2. Next, a more advanced model with the damping coefficient being a linear function for the displacement amplitude is introduced. The error now is less than 2% and energy dissipation recovery is almost perfect, see again Table 2. In general, a more complete model for nonlinear viscosity is possible, but it will necessarily be more complex and might depend on both loading and unloading phases, as well as on both the strain and strain-rate variation within a cycle of motion. Furthermore, for the purposes of engineering design, it is convenient to introduce the transmissibility function TR as the measure of the HDRB response. This function gives the ratio of the superstructure motion output (top surface of the HDRB) to ground motion input (bottom surface of the HRDB). The present work indicates that for HDRB isolators, it is necessary to introduce the nonlinear viscosity term to account for strain-rate dependence. More specifically, the response of the rubber constituent of the HDRB to harmonic loads is velocity dependent. For optimal design of a material with constant damping ratio, the velocity exponent n should be close to zero, and for frequency ratios smaller than critical point a and larger than critical point b. For intermediate frequency ratio values, exponent n should be close to unity, see Figs 9 and 10. If the damping ratio is larger than 0.45, then exponent n should be close to zero, for the entire range of Ω. Finally, for a material modelled by a constant exponent n, damping ratio should be close to unity, for frequency ratios smaller than critical point d. For large values of the frequency ratio, damping should be close to zero in all cases, i.e., damping is actually detrimental. Although not mentioned thus far, the TR also depends on the magnitude of the imposed external loads, which constitutes an extra design consideration. The above observations have design repercussions, because it is important to minimize the transmissibility function values across the entire frequency range of the harmonic load input in order to optimize BI design.

REFERENCES

[1] Bhuiyan, A. K., Y. Okui, H. Mitamura, T. Imai. A Rheology Model of

High Damping Rubber Bearings for Seismic Analysis: Identification of Nonlinear Viscosity. *International Journal of Solids and Structures*, **46** (2009), 1778–1792.

[2] Markou, A. A., G. Oliveto, A. Mossucca, F. C. Ponzo. Laboratory Experimental Tests on Elastomeric Bearing from the Solarino Project, Progetto di Ricerca, Report DPC – RELUIS, Italy, Potenza, University of Basilicata, 2014.

[3] Norton, F. H. The Creep of Steels at High Temperatures, New York, McGraw-Hill, 1929.

[4] Irgens, F. Rheology and Non-Newtonian Fluids, Heidelberg, Springer-Verlag, 2014.

[5] Besson, J., G. Cailletaud, J. L. Chaboche, S. Forest, M. Bletry. Non-Linear Mechanics of Materials, Heidelberg, Springer-Verlag, 2010.

[6] Dall' Asta A., L. Ragni. Experimental Tests and Analytical Model of High Damping Rubber Dissipating Devices. *Engineering Structures*, **28** (2006), 1874–1884.

[7] Kelly, J. M. Dynamic and Failure Characteristics of Bridgestone Isolation Bearings. Report No. UCB/EERC 91/04, CA, Berkley, Earthquake Engineering Research Center, 1991.

[8] Kelly, J. M., E. Quiroz. Mechanical Characteristics of Neoprene Isolation Bearings, Report No. UCB/EERC 92/11, CA, Berkley, Earthquake Engineering Research Center, 1992.

[9] Kelly, J. M. Earthquake-Resistant Design with Rubber, Heidelberg, Springer-Verlag, 1997.

[10] Naeim, F., J. M. Kelly. Design of Seismic Isolated Structures, from Theory to Practice, New York, John Wiley, 1999.

[11] Weisstein, E. W. Wallis Cosine Formula, From MathWorld-A Wolfram Web Resource, `http://mathworld.wolfram.com/WallisCosineFormula.html`, 2003.

[12] Soong, T. T., M. C. Constantinou. Passive and Active Structural Vibration Control in Civil Engineering, Vienna, Springer-Verlag, 1994.

[13] Hansen, N. The CMA-Evolution Strategy: A Tutorial, `https://www.lri.fr/~hansen/cmatutorial.pdf`, 2011.

[14] MATLAB, The MathWorks, Inc., Natick, Massachusetts, 2009.